Immunol Res (2013) 56:44–60
DOI 10.1007/s12026-013-8385-z

Theoretical analysis of the neuraminidase epitope of the Mexican A H1N1 influenza strain, and experimental studies on its interaction with rabbit and human hosts

Paola Kinara Reyes Loyola · R. Campos-Rodríguez · Martiniano Bello · S. Rojas-Hernández · Mirko Zimic · Miguel Quiliano · Verónica Briz · M. Angeles Muñoz-Fernández · Luis Tolentino-López · Jose Correa-Basurto

Published online: 1 February 2013

Abstract The neuraminidase (NA) epitope from the Mexican AH1N1 influenza virus was identified by using sequences registered at the GenBank during the peak of a pandemic (from April 2009 to October 2010). First, NA protein sequences were submitted for multiple alignment analysis, and their three-dimensional models (3-D) were then built by using homology modeling. The most common sequence (denominated wild-type) and its mutants were submitted to linear and nonlinear epitope predictors, which included the major histocompatibility complex type II (MHC II) and B-cell peptides. The epitope prediction was in accordance with evolutionary behavior and some protein structural properties. The latter included a low NA mutation rate, NA 3-D surface exposure, and the presence of high hindrance side chain residues. After selecting the epitope, docking studies and molecular dynamics (MD) simulations were used to explore interactions between the epitope and MHC II. Afterward, several experimental assays were performed to validate the theoretical study by using antibodies from humans (infected by pandemic H1N1) and rabbits (epitope vaccination). The results show 119 complete sequences that were grouped into 28 protein sequences according to their identity (one wild-type and 27 representative mutants (1–5 mutations)). The predictors yielded several epitopes, with the best fit being the one located in the C-terminal region. Theoretical methods demonstrated that the selected epitope reached the P4, P6,

Electronic supplementary material The online version of this article (doi:10.1007/s12026-013-8385-z) contains supplementary material, which is available to authorized users.

P. K. R. Loyola · M. Bello · L. Tolentino-López · J. Correa-Basurto (✉)
Laboratorio de Modelado Molecular y Bioinformática de la Escuela Superior de Medicina, Instituto Politécnico Nacional, México, Plan de San Luis Y Diaz Mirón S/N, Col. Casco de Santo Tomas, CP: 11340 Mexico city, Mexico
e-mail: corrjose@gmail.com; jcorreab@ipn.mx

P. K. R. Loyola
e-mail: dra.reyes.loyola@gmail.com

M. Bello
e-mail: bellomartini@gmail.com

R. Campos-Rodríguez · S. Rojas-Hernández
Departamento de Bioquímica y Sección de Estudios de Posgrado e Investigación, Escuela Superior de Medicina-IPN, Mexico, Mexico

M. Zimic · M. Quiliano
Bioinformatics Unit Faculty of Science and Philosophy, Universidad Peruana Cayetano Heredia, Av. Honorio Delgado 430, SMP, Lima, Peru
e-mail: mzimic@gmail.com

M. Quiliano
e-mail: mquiliano@alumni.unav.es

M. Quiliano
Drug R&D Unit, Center for Applied Pharmacobiology Research, University of Navarra, C/Irunlarrea s/n, 31008 Pamplona, Spain

V. Briz · M. A. Muñoz-Fernández
Laboratorio de Inmunobiología Molecular, Hospital General Universitario Gregorio Marañón, Networking Research Center on Bioengineering, Biomaterials and Nanomedicine (CIBER-BBN), Domicilio: C/Doctor Esquerdo no. 46, España, 28037 Madrid, Spain
e-mail: veronica.briz@gmail.com

M. A. Muñoz-Fernández
e-mail: mmunoz.hgugm@salud.madrid.org; mmunoz.hgugm@gmail.co

P7, and P9 pockets of MHC II, whereas the experimental evidence indicates that the epitope is recognized by human antibodies and also by rabbit antibodies immunized with the peptide.

Keywords Epitope vaccine · Neuraminidase · Prediction of immunogenic epitopes · Influenza AH1N1 · Docking · Molecular dynamics simulations

Introduction

The influenza virus responsible for the influenza epidemic (H1N1) affecting Mexico in April 2009 was a recombinant of genes from avian, swine, and human strains. Although the original host was swine, the virus was able to cross the species barrier and infect humans, subsequently resulting in human-to-human spread of the influenza virus [1]. The ability of the influenza virus to cross species barriers and to mix its genes in one host is the major reason why new strains emerge [2].

Influenza virus is a single-stranded RNA virus, and the virus has a high antigenic variability of different types of genetic events (antigenic shift, antigenic drift, recombinant, and redistribution). The replication strategy of single-stranded RNA viruses is prone to errors, exhibiting one error per replication [3, 4]. Under these conditions of genetic mixing and a rapid mutation rate, there is a great significant probability that many virulence factors can be combined, leading to new strains that produce a high morbidity and mortality in human populations, as demonstrated by the 2009 pandemic in Mexico [5].

The influenza virus contains two cell surface glycoproteins, hemagglutinin (HA), and neuraminidase (NA), which are keys to host infection. HA binds to the sialic acid present on the surface receptors of upper respiratory epithelial cells, whereas NA enables new virus copies to escape from these host epithelial cells. These glycoproteins cleave the poly-sialic acids, releasing new virions into the host cells [6]. Although it is known that both proteins play important roles in the life cycle of the influenza virus [6], in this contribution, we only explored the NA epitopes because they are one of the most important protective antigens of AH1N1. However, at the present time, a similar study focused on HA is being performed by our research group, which will be published elsewhere.

The location of HA and NA on the viral capsid renders the virus susceptible to immune recognition [7]. This property is the basis for the design of current influenza vaccines, and anti-influenza drugs work mainly by interfering with the functions of these two proteins [8]. However, most of the present vaccines currently available are designed to activate the adaptive immune system by allowing it to recognize many virus strains, but in some cases, they do not cross-react with emerging strains. In addition, there are some influenza virus vaccines that yield undesirable reactions during their application [9]. Thus, to avoid undesirable reactions, peptide-based vaccine approaches have been explored. In addition, an increase in the immunological response of peptides can be reached by using a protein known as keyhole limpet hemocyanin (KLH) as an adjuvant. KLH is a potent immunostimulating protein with an extensive history of safe and effective use in vaccine development and immunological research [10].

There are several methods to identify epitopes for vaccine design. One method involves the use of computation tools; however, this method is employed in a limited fashion [11]. There are computational methods that use only protein sequences to identify possible epitopes [12]. In contrast, the docking [13] and molecular dynamics (MD) methods [14] could be used to determine whether the protein complexes are maintained after epitopes reach the major histocompatibility complex (MHC) type II [15].

Therefore, we identified NA epitopes by employing a combination of methods, beginning with traditional epitope predictors, and refining the results with docking and MD studies. In this work, we analyzed the pandemic influenza virus AH1N1 that affected Mexico in 2009 [16] and identified highly immunogenic epitopes of NA. Moreover, we validated these theoretical studies with experimental data, performing recognition assays with human antibodies (Ab) from patients infected with the pandemic virus in Mexico. Finally, we administered epitopes (alone or conjugated with keyhole limpet hemocyanin (KLH)) to rabbits, and their Ab were then submitted against the peptide alone or conjugated with KLH for experimental recognition studies.

Materials and methods

Theoretical procedure

Protein sequence search and multiple sequence analysis

We searched, and submitted for multiple sequence alignment, the NA protein sequences found in the pandemic virus from Mexico (April 2009 to October 2010), which are indexed in the GenBank database, using STRAP (Structure-based Sequence Alignment Program) [17] to identify the NA-mutated and NA-conserved regions.

Homology modeling

The Swiss-Model (http://swissmodel.expasy.org/) server was used for the homology modeling of the most common (denoted wild-type) and representative mutants [18–20]. The NA crystal structure of the AH5N1 strain (PDB ID:

2HTY) was employed as a template. The structures obtained in this manner (intramembrane domain: 1–82 amino acids and C-terminal domain: 2 amino acids) were completed using the Modeller (http://www.salilab.org/modeller/) program [21]. It is important to mention that during the development of this study and the writing of this article, the three-dimensional NA structure for the influenza virus responsible for the 2009 AH1N1 pandemic was published [22]. This new crystal structure is indexed at the Protein Data Bank (PDB ID: 3NSS). We compared the modeled three-dimensional structures, wild-type and 3NSS, and found that they overlap, both sharing the same protein sequence. Moreover, to validate our models, we used a docking procedure that our group has utilized in other reports [23], employing a known ligand (oseltamivir). Docking studies are widely used for validating three-dimensional models built elsewhere [24]. Therefore, we employed docking simulations with oseltamivir on each of the 28 NA three-dimensional structures. These results reproduced the binding pose on our wild-type NA, as has been reported previously [25], but displayed a different behavior on mutated NA structures.

Prediction of immunogenic epitopes (MHC II and B-cell epitopes)

Four programs were used for epitope predictions: the ProPred (http://www.imtech.res.in/raghava/propred/) and MHC2Pred (http://www.imtech.res.in/raghava/mhc2pred/info.html) programs for the MHC II–epitope predictions, and the CEP (http://bioinfo.ernet.in/cep.htm) and ElliPro (http://tools.immuneepitope.org/tools/ElliPro) programs for the B-cell–epitope predictions. ProPred predictions are based on locating the promiscuous regions that can bind HLA-DR alleles [26], including the 47 HLA-DRB1s, which are the most representative. Furthermore, because in this study we focused on MHC II, known to bind to peptides that are 10–40 amino acids long with a binding core of nine amino acids, predictions with MHC2Pred were made for these core nonamers. Each peptide was represented as a 20-dimensional vector (SVM) using 12 alleles of its matrix (10 HLA-DRB1, 1 HLA-DRB5, and 1 HLADRB4) [27].

The CEP program, used for B-cell epitope predictions, possesses an algorithm that employs a structure-based bioinformatics approach and solvent accessibility of amino acids in an explicit manner [28]. ElliPro implements three algorithms that perform the following tasks: (1) approximation of protein shape as an ellipsoid, (2) calculation of the residue protrusion index (PI), and (3) clustering of neighboring residues based on their PI values [12]. To select the best epitope from the protein sequence predictions, both the epitope predictor results and the three-dimensional criteria were taken into account. Furthermore, we considered the following criteria: (1) the best score from the predictor (except for predictions by CEP), (2) the common epitope that was predicted from the four predictors, (3) the protein surface location (considering only the loops outside the internal protein location and not the transmembrane domains, beta sheets or alpha helices), (4) the exposure of an epitope that could easily be reached by an antibody, and (5) the low rate of mutations exhibited by the epitope.

Docking the predicted epitope on molecular histocompatibility complex type II

Once the best *predicted* epitope was selected, a docking study was employed to illustrate the epitope and MHC II interactions. We selected the HLA-DRB1*0401 (PDB ID: 1D5M) crystal structure of MHC II because some experimental data and computational predictions have demonstrated that this structure is related to the response of the influenza AH1N1 virus [29]. Moreover, this HLA-DR allele is present in the majority of humans [30]. To observe how our theoretical procedure compared with the experimental data, an epitope co-crystallized with MHC II (PDB ID: 1D5M) was re-docked using the Autodock 4.0.1 program [31], which has been employed in other reports [32].

The search space was restricted to a rectangular box that included β-folded chains and α-helix chains, targeting the binding site of the predicted epitope and MHC II. A rectangular grid (70 × 100 × 90 Å) with points separated by 0.375 Å was generated. The docking parameters used were 100 runs, with 100 million energy evaluations for each test, and a population size of 100 individuals [31]. The peptide was treated as flexible, allowing it to experience conformational changes on the MHC II-binding site. The docking results were analyzed using Autodock Tools software version 1.5.0 [31].

Molecular dynamics simulations

MD simulations were performed using NAMD 2.6 [33] with the CHARMM27 force field [34]. First, the system was embedded in a solvated water box and neutralized with 23 Na^+ atoms. All water molecules were closer to 3.8 Å than to any atoms of the protein that did not possess hydrogen atoms. Prior to the MD simulations, the system underwent an equilibrium process, which started with an initial minimization, with all backbone atoms fixed. Afterward, the system (without restrictions) was heated with short MD simulations (30 steps), which were then continued under the NTP protocol to reduce anomalous initial contacts and to fill the empty spaces. A 30-ns-long

MD simulation was performed under NTV assembly to execute the structural analyses.

All simulations were performed on a Linux cluster of 19 nodes with 4 cores each. The trajectory data were saved every 2 ps and subsequently analyzed using the CARMA program [35]. All snapshots for the epitope–MHC complex were taken at 1-ns intervals, and they were then visualized using the visual molecular dynamics (VMD) program [36]. In addition, the CARMA program [35] was used to obtain root-mean-square deviations (RMSD), the root-mean-square fluctuations (RMSF), and the radius of gyration (Rg).

Experimental procedures

Rabbit immunization

Two rabbits were immunized, one with peptide–KLH and the other with the peptide alone, on three different days. On day 1 (first immunization), 1 mg of peptide plus complete Freund's adjuvant (Sigma Chemical Co.) was administered through the subcutaneous route. On day 8 (second immunization), 1 mg of peptide plus incomplete Freund's adjuvant was administered through the subcutaneous route. On day 15 (third immunization), 1 mg of peptide in 5 mL of saline solution was administered through the intramuscular route. Seven days after the last immunization, the rabbits were anesthetized with pentobarbital, and serum samples were obtained from blood extracted by cardiac puncture and stored at −70 °C.

Biological samples

Blood and saliva were obtained according to previously reported procedures [37] from healthy individuals who were living in Mexico City during the peak of the influenza H1N1 virus pandemic in 2009 [16]. The samples were divided into aliquots of 500 μL and stored at −70 °C.

Detection of rabbit and human IgG using the neuraminidase peptide

Anti-neuraminidase peptide levels were evaluated in serum samples from the immunized rabbits and from infected and asymptomatic individuals. The Ab levels in the serum samples were determined using an indirect enzyme-linked immunosorbent assay (ELISA). Briefly, 96-well plates were coated with either peptide–KLH or peptide alone (2 μg of peptide/mL) in carbonate bicarbonate buffer (15 mM Na_2CO_3, 35 mM $NaHCO_3$, at pH 9.6). The plates were incubated for 2 h at 37 °C and washed three times with 0.05 % Tween-20 in PBS (PBST). Blocking was performed by treating with PBST plus 6 % fat-free milk and by further washing with PBST. Each sample was tested in duplicate. Serum samples from immunized rabbits were diluted 1:1,000, 1:2,000, 1:4,000, 1:8,000, and 1:16,000. Serum samples from individuals were diluted 1:50 or 1:100. After the plates were incubated overnight at 4 °C and washed with PBST, 1:1,000, 1:2,000, and 1:4,000 dilutions of goat anti-mouse IgG (Santa Cruz Biotechnology) or rabbit anti-human IgG (1:1,000, Santa Cruz Biotechnology) were added to each well, and the plates were incubated for 2 h at room temperature. The plates were washed with PBST, and the enzymatic reactions were started by adding substrate solution (0.5 mg of o-phenylenediamine/mL plus 0.01 % H_2O_2 in 0.05 M citrate buffer at pH 5.2). After 15 min, the reactions were stopped with 25 μL of 2.5 M H_2SO_4, and the absorbance at 492 nm (A 492) was measured using a Multiscan Ascent (Thermo Labsystems) microplate reader.

Detection of the neuraminidase peptide using an immunodot assay

Peptide–KLH or peptide alone (10 μg) was impregnated on nitrocellulose membrane strips for 30 min at room temperature. Afterward, the strips were washed three times with PBST and blocked by incubating with PBS containing 10 % nonfat dry milk at pH 7.4 for 1 h. The strips were then incubated with rabbit serum at a dilution of 1:100 anti-peptide–KLH, or anti-peptide alone with human serum at a dilution of 1:10 and with undiluted saliva, followed by washings with PBST. Finally, the strips were incubated for 1 h with the peroxidase antibodies at a dilution of 1:1,000. Goat anti-mouse IgG or goat anti-human IgG antibodies were used for strip incubations with serum, whereas anti-IgA antibodies were used for strip incubations with saliva (Santa Cruz Biotechnology). After the incubation period, the strips were washed with PBST, and the recognized proteins were revealed with substrate solution (H_2O_2, 3.6 mM 4-chloro-1-napthol; Pierce, Rockford, IL, USA).

Statistical analysis

Kruskal–Wallis (nonparametric) tests were used for comparing results from different groups. The significance of differences between the groups was assessed using a Mann–Whitney unpaired, two-tailed test. The tests applied are indicated in the figures. All analyses were performed using commercial computer programs (Sigma Plot 11, SPSS Inc).

Table 1 Twenty-eight representative protein sequences for NA AH1N1, including 1 wild-type (WT) and 27 representative mutants (numbered from 1 to 27), are listed

ps	WT	1	2	3	4	5	6	7	8	9	10	11	12	13	14
aa															
I23		M													
I30			T												
I34				P											
S35				V	G										
H36						R									
N42							D								
V83				M				M	A	A					
G77											R				
K84												T			
A86													V	V	
S95				G				G							G
S105															
V106			I				I			I		I		I	
P126					H				I						
E128											G				
G147							E								
N189															
N248			D				D		D	D		D		D	
H274															
H275															
S286															
S366									N						
G382															E
I389															
N397							S								

ps	15	16	17	18	19	20	21	22	23	24	25	26	27
aa													
I23													
I30													
I34													
S35													
H36													

Table 1 continued

ps	15	16	17	18	19	20	21	22	23	24	25	26	27
N42													
V83													
G77													
K84													
A86	G												
S95		N											
S105		I	I	I	I	I	I	I	X	X			
V106													
P126													
E128													
G147													
N189			S		D	D							
N248		D	D	D			D	X	X	D	D		
H274					Y								
H275						Y							
S286												G	
S366							N						
G382													
I389													T
N397													

In the left column, amino acid residues that have mutations are indicated. The positions of the mutations are defined (top row), and the corresponding amino acid (aa) replacement is indicated

Results and discussion

Theoretical results

In October 2010, protein searches yielded 182 sequences, of which 119 were complete and 63 were incomplete (supplementary material). The complete sequences were identified using multiple sequence analysis, as previously described [38, 39]. To assure a detailed structure, only complete protein sequences were considered.

Beginning with the NA sequences retrieved from the GenBank database, multiple sequence alignments showed 28 NA groups, including 27 NA mutants and one wild-type NA. The NA mutants had between 1 and 5 mutations (Table 1 and supplementary material), most of which were point mutations. Only two protein sequences were deletions. Interestingly, the last 20 amino acid residues in the C-terminal domain were conserved (Fig. 1; Table 1).

Only 3 NA sequences had the H274Y mutation, which is associated with oseltamivir resistance [25]. Although the H274Y mutation is located outside the catalytic site, it increases the hindrance effect of Glu274, thus repelling the hydrophobic moiety of oseltamivir [25, 40]. Although NA mutations at catalytic sites are rarely reported [41], our results demonstrate an increase in mutations at catalytic sites, which is in agreement with other studies [42]. Furthermore, there are recent reports on D198N, S248N, and K261R mutations, which confer resistance to oseltamivir, and Y155H and S246N mutations, which present resistance to oseltamivir and zanamivir [42]. The C-terminal region obtained from multiple sequence analysis is an optimal region to search for immunogenic epitopes because these sequences have been reported as highly conserved not only in H5N1 NA but also among the NAs of the influenza A subtypes H1N1, H3N1, H4N1, H6N1, H7N1, H9N1, H10N1, H11N1, and H12N1 [43].

After selecting the NAs and grouping them based on NA mutations, we used theoretical predictions to search for MHC II and B-cell epitopes (see the "Materials and methods" section). These epitope predictors were selected because they have been widely used to identify antigens (Ag) that create humoral responses for vaccination purposes [44] and are commonly used in the field of immunology for vaccine design [45]. These predictors have been shown to decrease the costs of vaccine development and to avoid the unwanted responses that occur with vaccines derived from attenuated pathogens, whether alive or dead [46].

As previously mentioned, both the epitope predictor results and the three-dimensional criteria were taken into account for the purpose of identifying epitopes. After all the three-dimensional NA structures considered were built and validated, several epitopes were identified in different NA regions (Fig. 2), which were then submitted to the five

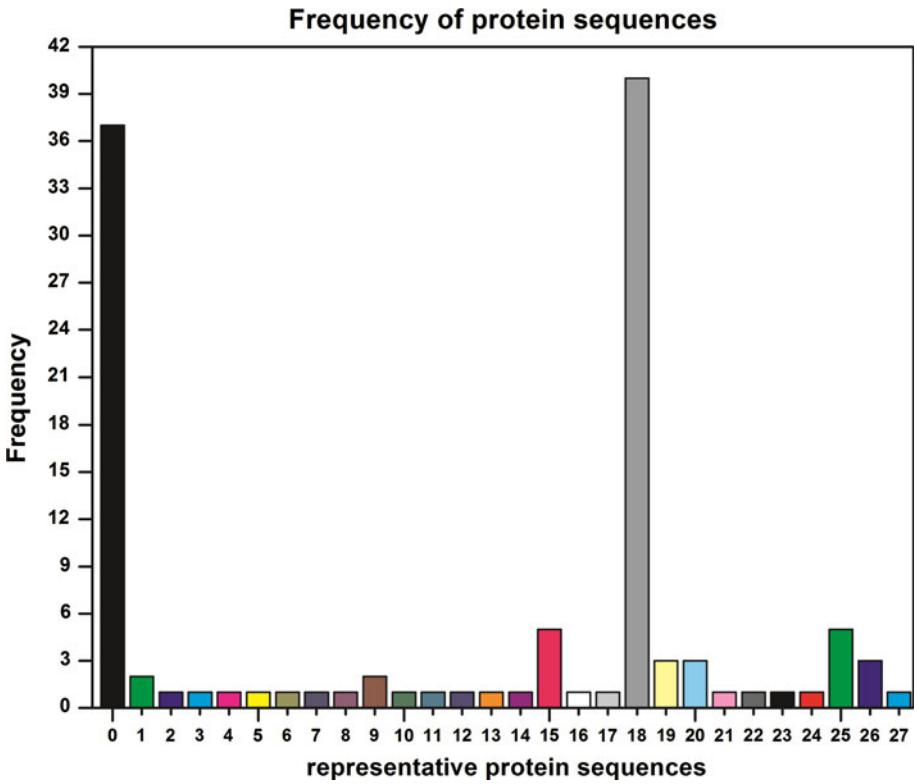

Fig. 1 Frequency of the 28 representative sequences obtained by multiple sequence analysis. The 27 protein sequences with mutations are represented in *different colors* and WT (0) in *black*, with the corresponding mutation frequency on the side (Color figure online)

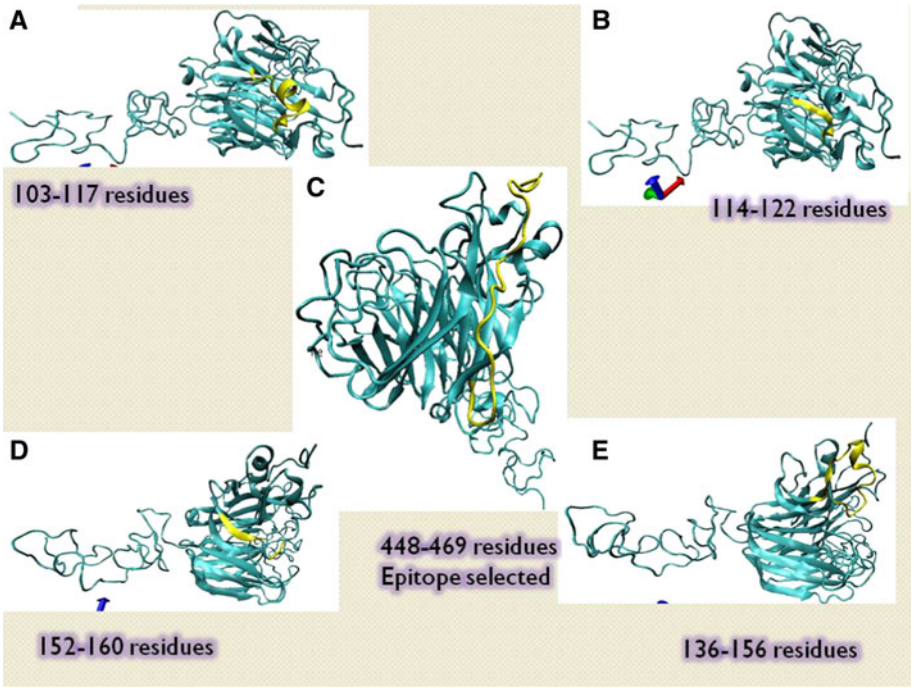

Fig. 2 Three-dimensional structures of the immunogenic peptides used by representative NA reported in Mexico during the pandemic virus (homology modeling). In **a**, **b**, **d,** and **e**, the tertiary structures of predicted peptides are shown: **a** Peptide 103–117 is in α-helix; **b** Peptide 114–122 is in β-fold; **c** The predicted epitope by the five criteria used, selected in conjunction with 3-D analysis; **d** The peptide 152–160 is in β-fold; **e** The peptide 136–156 is in β-fold

Table 2 Prediction results for the peptide–MHC II complex from ProPred and MCH2Pred servers

Peptides conserved and located on the protein surface are indicated. Both servers predicted the selected peptide that ranges from 447 to 455 amino acids

ProPred			MCH2Pred		
Number of residues	Sequences	Score	Number of residues	Sequences	Score
105	VRIGSKGDV	4.9	–	–	–
114	FVIREPFIS	6.2	113	VFVIREPFI	0.584
131	FFLTQGALL	6.0	130	TFFLTQGAL	1.389
154	YRTLMSCPI	4.6	151	RSPYRTLMS	0.768
447	VNSDTVGWS	5.3	447	VNSDTVGWS	0.749

structural epitope criteria previously described. For each structural criterion, epitopes with the best scores were selected with the aim of selecting the most antigenic agents.

The three-dimensional structure criteria allowed us to discard epitopes located in intra-protein and transmembrane domains because antibody interactions with these protein surfaces are difficult. The epitopes located in alpha helix and beta folded regions were also discarded because these regions are difficult to fit with antibodies. Ab with loops or terminal tails do not have difficulty reaching these regions if they are stable [47, 48]. Finally, the multiple alignment studies allowed us to discard NA regions with high substitution rates because it is known that such regions, which have antigenic properties [49], prevent contact between the Ab and the virus [50]. Among all the NA epitopes identified by the predictors (Table 2), the predicted epitope was the only one that fit all the criteria used. The other epitopes were discarded because they were located on the alpha or beta secondary structures of the NA.

The predicted epitope that was selected contains 22 amino acid residues (448VNSDTVGWSWPDGAELPF-TIDK469) and is located at the C-terminal region (Fig. 2c). It has a core of nine amino acid residues, as predicted by the epitope–MHC II predictors, which are the residues considered for epitope–B-cell predictors (Table 2). Previous multiple alignment studies indicate that the predicted epitope is located in a highly conserved C-terminal domain of NA [43], in agreement with our results. Our analysis showed that the predicted epitope is located in an exposed region of the NA and therefore has surface accessibility (as indicated by the CEP predictor, Fig. 2c). By using three-dimensional structures, it is possible to identify whether epitopes are in a loop or tail to identify which epitopes have sufficient mobility to reach the MHC II [51] or an Ab for recognition [52]. The selected epitope has the

Table 3 Predictions for the peptide–B cell complex from CEP and ElliPro servers

CEP		ElliPro	
Number of residues	Sequences	Number of residues	Sequences
107–113	RIgSKGD	103–117	DNSVRIGSKGDVFVI
142–155	DKHsNGtIKDRSPY	136–156	QGALLNDKHSNGTIKDRSPYR
449–469	NSDTVGWSwPdGaEIPfTIDK	448–469	VNSDTVGWSWPDGAEIPFTIDK

Peptides conserved and located on the protein surface are indicated. Both servers predicted the selected peptide that ranges from 449 to 469 amino acids

advantage of being highly conserved, which enables a cross-immune response [43]; moreover, it contains three aromatic residues and a heterogeneous structure that confers immunological properties [53]. The selected peptide also contains a high percentage of hydrophobic residues (43 % hydrophobic, 17 % acidic, 4.35 % basic, and 34 % neutral residues), which have been implicated in immunogenic properties [54]. Additionally, the selected epitope is not likely to induce an autoimmune response in humans, evidenced by the fact that a low identity was found between this predicted epitope sequence and human protein sequences when using a Basic Local Alignment Search (BLASTP; http://blast.ncbi.nlm.nih.gov/; Table 3).

With docking simulations, we produced an epitope–MHC II complex and identified several important interactions that suggest a stable MHC II–epitope complex [55]. The docking studies demonstrate that the predicted epitope that was selected reaches MHC II (Fig. 3) through its reported pockets (P), which are characterized by accepting key amino acid residues that stabilize the complex [56]. It is important to mention that the docking procedures do not consider several biological conditions, which are taken into account in MD simulations [57]. Therefore, the epitope–MHC II complex obtained by docking simulations was refined by MD simulations, as has been performed in previous analyses [58].

To examine the contacts between the predicted epitope and MHC II by MD simulations, we analyzed structural protein movements, depicted in the RMSD values, to evaluate when the system reaches convergence. This analysis indicated that the NA indeed reached convergence at 3 ns and remained stable during the remainder of the MD simulations (Fig. 4a). In other reports using theoretical procedures, experimental procedures, and protein dimers, convergence was reached in a shorter period of time (first ns) [59], confirming the time of 3 ns found in the present study, and the Rg and the RMSD displayed the same behavior during the MD simulations (Fig. 4a, b). The RMSF values that were retrieved from the MD simulations indicate the behavior of the backbone residues and demonstrate the stability of the proteins (Fig. 4c, e, f) [60]. The RMSF values, in relation to either the predicted epitope or

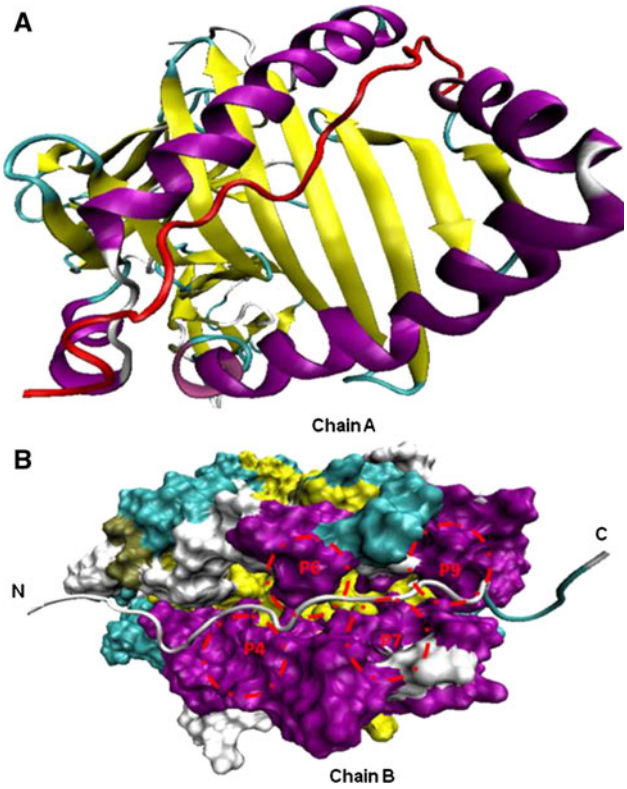

Fig. 3 **a** The docking models of the peptide–MHC II complex with stabilized pockets are depicted in the cartoons. **b** Surfaces of MHC II that make contact with the peptide are illustrated. The pockets reached by the peptide are circled in *red* (Color figure online)

MHC II, demonstrated a greater motion in zones that do not have contact, whereas there were fewer fluctuations at the contact surfaces. All these indicators suggest that the epitope–MHC II interactions are stable (Fig. 4c, e, f), corroborating the docking studies. Before performing the docking of the target epitope and MHC, a docking study was conducted using the co-crystallized form of 1D5M, displaying a free energy of −7.27 kcal/mol and an RMSD of 3.86 Å (data not shown).

Due to the chemical contacts between the pockets of the MHC II and the predicted epitope, the formation of a stable epitope–MHC II complex is a necessary step to induce a specific immune response because this complex enables Ag

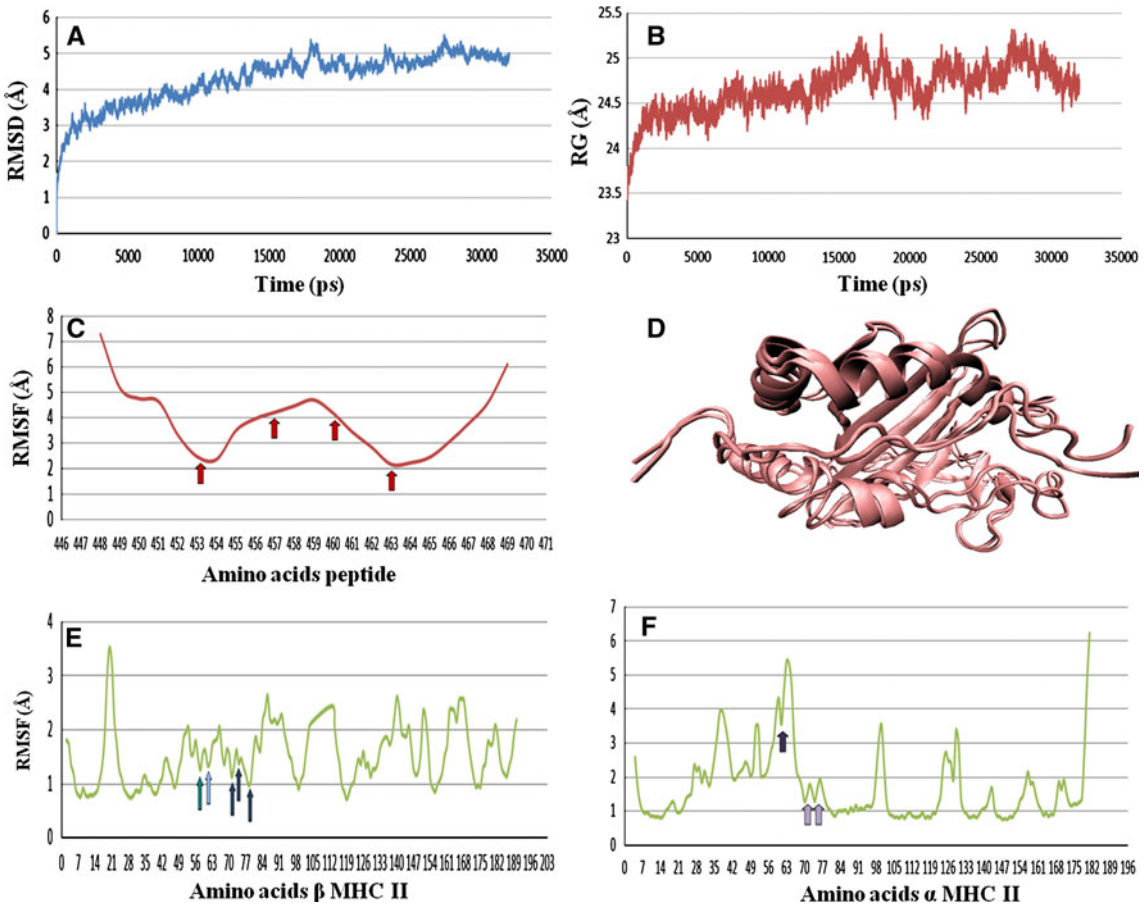

Fig. 4 **a** Root-mean-square deviations (RMSD) of the peptide–MHC II complex during MD simulations (30 ns); **b** Radius of gyration (Rg) of the epitope–MHC II complex during MD simulations (30 ns); **c**, **e**, and **f** Root-mean-square fluctuations (RMSF) of the epitope residues that interact with the α and β chains of MHC II are depicted; **c** Epitope residues are labeled with *red arrows* (Leu463, Gly460, Trp457, and Thr453); **d** Complex of MHC II and epitope at 0 ns and end of MD simulations time; **e** *Arrows* mark residues that interact with the β chain of MHC II. A seawater *arrow* marks the residue of P9 (βAsp57), a *light blue arrow* marks residues of P7 (βTrp61), and *dark blue arrows* mark the residues of P4 (βGln70, βAla74, and βTyr78). **f** For the α chain of MHC II, *dark purple arrows* mark residues of P6 (αAsn62), and *light purple arrows* mark residues of P9 (αArg76, αIle72) (Color figure online)

presentation to T-cell receptors [61, 62]. Several snapshots were retrieved to identify the binding pose of the predicted epitope on MHC II, indicating that the predicted epitope reaches the P4, P6, P7, and P9 pockets (Fig. 5). The MHC II pockets (P1-11) are very important for epitope recognition [56], particularly the P1 pocket [55]. Several authors have reported that binding at P1 plays a very important role in the stabilization of the epitope–MHC II complex after the epitope is reached by Trp, Tyr, Phe, Leu, and Ile [63]. Nevertheless, the docking and MD simulations from our study do not indicate that the predicted epitope reaches P1 (Fig. 5) but rather that other MHC II pockets are, in fact, more important [58, 64].

The docking and MD simulations indicate that Leu463 of the predicted epitope interacts with the P4 pocket, mediated by a hydrogen bond with βGln70 and by Van der Waals forces with βTyr78 (Fig. 5a). In addition, Trp457 of the predicted epitope reaches the P7 pocket through π–π interactions with βTrp61 (Fig. 5d), which is consistent with the literature [56].

The P6 and P9 pockets are other important recognition sites within MHC II. It is well known that the interactions of certain residues in P6 modify the conformation of P9. For example, the binding of positively charged residues at P6 can reduce the P9 cavity, limiting the ability of this pocket to interact with residues that have hydrophobic side chains. In contrast, the binding of negatively charged residues at P6 enlarges the P9 cavity, enabling this pocket to accept residues with larger side chains [64].

Gly460 was identified in our study as the residue closest to P6 (Fig. 5b). This residue creates a negative environment and generates a conformational change in P9, which allows P9 to accept residues with larger side chains, such as Thr452 and Val453 (Fig. 5c, e). The interaction of the Gly460 backbone with the αAsn62 carbonyl backbone of P6 is mediated through hydrogen bonds (Fig. 5b). There

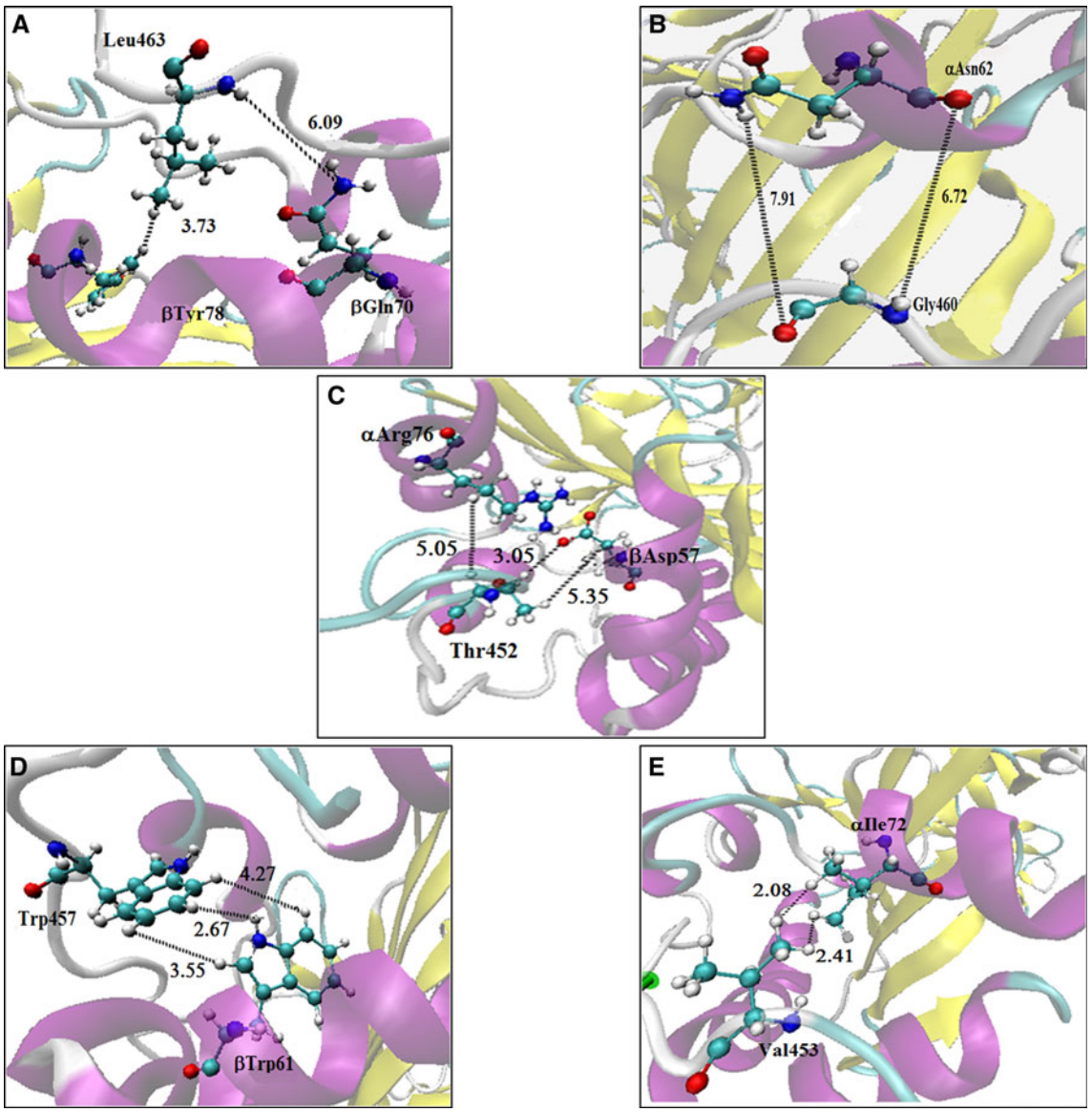

Fig. 5 Illustration of the interactions between residues of pockets of MHC II and residues of the peptide (transparent 3-D cartoon). **a** Interactions at P4 are illustrated; the opaque color marks residues (βTyr78 and βGln70) that interact with Leu463 of the peptide; **b** The residues at P6 (αAsn62) that interact with Gly460 of the peptide are depicted in the opaque colors; **c** The residues at P9 (αArg76 and βAsp57) that interact with Thr452 of the peptide (opaque) are marked; **d** Interactions at P7 are illustrated; the residues (opaque) mark contacts between βTrp61 and Trp457 of the peptide; **e** The interaction between P9 (αIle72) and Val453 of the peptide is marked (opaque)

are other interactions between the predicted epitope and MHC II that are also mediated through hydrogen bonds, such as those between Thr452 of the epitope and αArg76 and βAsp57 of P9. Finally, another important interaction exists between αIle72 of P9 and Val453 of the epitope through hydrophobic contacts (Fig. 5e).

RMSF can be used to show the motion of the backbone alpha carbon of residues during the MD simulations. This motion is important because there is evidence to indicate that lower motions depict epitope–MHC II complex stability. In general, the RMSF values found in our study suggest that the interactions with the MHC II pockets are stable in comparison with those residues that are not making interactions, the latter of which reached RMSF values close to 7 Å. For example, the RMSF values for the epitope residues that interacted with the MCH II pockets (P4, P6, P7, and P9) were as follows: Leu463, 2 Å; Gly460, 3 Å; Trp457, 4 Å; and Thr453, 2 Å. The RMSF values of αArg76, αIle72, βGln70, βAla74, βTyr78, βTrp61, and βAsp57 were the lowest (1–2 Å). In contrast,

the RMSF values (Fig. 4c, e, f) indicate that residue αAsn62 of MHC II shows the highest degree of motion (3.8 Å) because this residue interacts with Gly460 of the peptide, the latter of which is a residue without a side chain; that is, P6 was empty and its constituent residues were moving to interact with Gly460 of the peptide. It is also important to mention that αAsn62 is located in a short α-helix between two very flexible loops (4.2 and 5.4 Å; Fig. 4f).

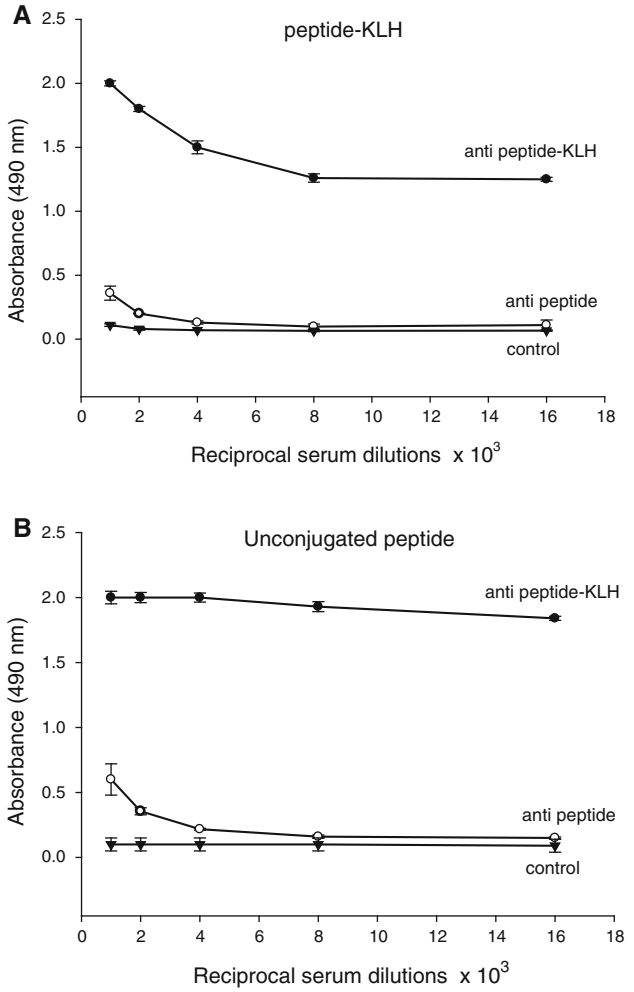

Fig. 6 Detection of rabbit IgG Ab to the neuraminidase peptide by ELISA. Serial dilutions of sera from rabbits inoculated with unconjugated peptide or the peptide conjugated to KLH were added to microplates previously coated with peptide–KLH (**a**), peptide alone (**b**), or a peptide of hemagglutinin (**c**). Serum from rabbit immunized with *Naegleria lovaniensis*, a peptide unrelated to the pandemic influenza strain, was used as the control. *Bars* represent the mean absorbance values ± standard deviations (SD) for Ab levels from each experimental group. The IgG Ab to the neuraminidase peptide was detected with a secondary Ab specific for rabbit IgG. Results are expressed as the mean absorbance ± SD. The serum from rabbit immunized with peptide–KLH showed the highest titer (1:16,000), whereas the serum anti-peptide had a lower titer (1:2,000)

With the results obtained from the docking and MD simulations, it can be suggested that MHC II is able to recognize the epitope selected in this study and that this epitope–MHC II complex is stable over the entire MD simulation. This stability is essential for the creation of an antigen-specific immune response [56, 61, 65].

Experimental results

Enzymatic immunoassays were performed to confirm that the selected peptide is immunogenic and antigenic. First, the peptide's immunogenicity and antigenicity were analyzed using immunizing rabbits with the peptide alone or with the peptide conjugated to KLH in complete Freund's adjuvant (CFA) and then by quantifying the antibodies by ELISA. In the ELISA assay, the plates were coated with either the peptide coupled to KLH (peptide–KLH) or the unconjugated peptide.

As expected, the IgG Ab in the rabbit serum was able to recognize the peptide or peptide conjugate (in the animal immunized with the peptide alone, Fig. 6, panel B, and in the animal immunized with the peptide plus KLH, Fig. 6, panel A, respectively). However, the titers of IgG Ab to the peptide were significantly higher in the serum of the rabbit immunized with the peptide conjugate (peptide–KLH). Thus, the serum anti-peptide–KLH contained IgG antibodies that disappeared at a dilution of 1/16,000, whereas in the serum anti-peptide alone, the IgG antibodies disappeared at a dilution slightly higher than 1/2,000.

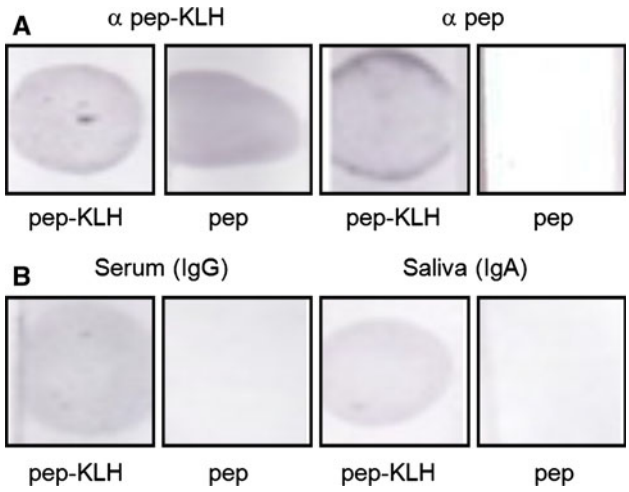

Fig. 7 Immunodot blot assay for the detection of the rabbit and human Ab to the neuraminidase peptide. **a** The rabbit antiserum (IgG Ab) to the peptide conjugated to KLH (α pep-KLH) recognized the conjugated (pep-KLH) and non-conjugated peptide (pep). The rabbit antiserum to the non-conjugated peptide (α pep) recognized the conjugated but not to the non-conjugated peptide. **b** IgG antibodies in human serum and IgA Ab in saliva recognized the conjugated (pep-KLH) but not to the non-conjugated peptide

The peptide alone induced IgG Ab in the absence of a carrier molecule, the latter of which is essential to induce a humoral immune response to small peptides. In other words, the peptide is highly immunogenic. In addition, the serum from the immunized rabbits did not recognize peptides from the B chain of the hemagglutinin peptide (data not shown), indicating that the Ab to the NA peptide were specific.

The immunogenicity and antigenicity of the peptide were also confirmed using an immunodot blot assay (Fig. 7). The IgG Ab of the rabbit immunized with the peptide plus KLH recognized the conjugated and unconjugated peptides. However, the IgG Ab of the rabbit immunized with the unconjugated peptide recognized only the peptide and not the conjugate (Fig. 7a). These results demonstrate that the peptide alone or coupled to a carrier is highly immunogenic. Notably, the peptide alone was also immunogenic and antigenic, despite being a small peptide (22 amino acid residues) weighing approximately 2,100 Daltons.

Finally, to determine that the peptide was antigenic in humans, the binding of human Ab (IgG and IgA) to the peptide was analyzed by ELISA and immunodot blot assay. Using ELISA, the unconjugated peptide and conjugated peptide were recognized by the IgG Ab in the sera of subjects who were living in Mexico City during the peak of the H1N1 pandemic in 2009 (Fig. 8). The IgG Ab in serum and IgA Ab in saliva also recognized the conjugated peptide, but not the unconjugated peptide, by immunodot blot (Fig. 7b). These results demonstrate that clinical or subclinical infections with the influenza virus induced IgG and IgA Ab to the peptide. Thus, the peptide is also immunogenic and antigenic in humans.

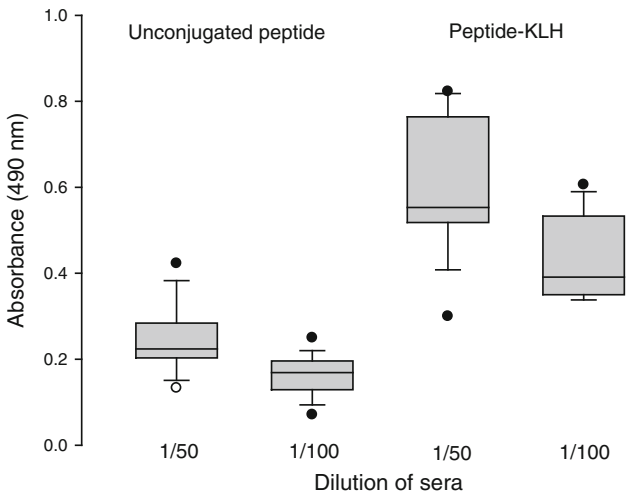

Fig. 8 Detection of human IgG Ab to the neuraminidase peptide by ELISA. Microplates were coated with peptide–KLH (*panel A*) or unconjugated peptide (*panel B*), and two dilutions (1/50 and 1/100) of sera from asymptomatic individuals were added and incubated at 4° C for 18 h. The IgG Ab to the neuraminidase peptide was detected with a secondary Ab specific for human IgG. Results are presented as *box and whisker plots*. The *boxes* define the 25th and 75th percentiles with a line at the median, with *error bars* defining the 10th and 90th percentiles and *circles* representing individual outliers. IgG Ab in human serum recognized both the unconjugated peptide and the conjugated peptide (peptide–KLH). The levels were significantly higher with the conjugated peptide ($P > 0.001$, Mann–Whitney rank sum test)

This peptide is a good immunogen because it induced an antibody response in rabbits. This immunogenicity could be based on several properties, such as molecular size, rigidity, chemical complexity, interaction with B-cell receptors, interaction with MHC, and activation of helper T cells [66]. Additionally, the peptide proved to be an Ag that is recognized by the IgG Ab from immunized rabbits and infected individuals, as has been reported for other peptides [61, 67–69]. However, to serve as an Ag, a substance typically must have a relative molecular mass of at least 4,000 Daltons, and the peptide under study is ~2,000 Daltons (21 amino acid residues). Interestingly, this peptide is one of the few substances with a low molecular weight (below 2,000) to have antigenic properties [70]. This peptide likely has a stable conformation or a rigid structure because its antigenic determinant (or epitope) requires it to have a consistent shape with a charge pattern that is recognized by a specific combined structure (e.g., an antibody or B-cell receptor) [71].

The immunogenicity of the peptide indicates that it must be relatively stable in solution. Although peptides are intrinsically disordered and, therefore, less stable than the full protein, the peptide under study is capable of adopting a conformational structure recognizable by combined Ab sites on B cells. It is also possible that the peptide is capable of adopting stable structures that mimic those found on the native protein. This idea is supported by MD simulations on the peptide, which demonstrated that the peptide maintains its secondary structure and has a low degree of motion, retaining some of the stability present in the native protein. Thus, for use in a vaccine, the peptide has significant advantages because its low structural movement allows antibodies to reach the peptide. Interestingly, this peptide possesses the complex chemical properties required to be immunogenic: it is composed of 43 % hydrophobic, 17 % acidic, 4 % basic, and 34 % neutral residues, resulting in a total of 14 % aromatic and 86 % nonaromatic residues.

It is also possible that the peptide's immunogenicity is related to its amino acid composition, its diversity of amino acids, and its ratio of aromatic to nonaromatic amino acids (14/86 %). Although the peptide contains few aromatic residues, one (Trp457) reaches P7 of MHC through π–π interactions with βTrp61 (Fig. 5d). However, the docking and MD simulations show that the peptide reaches other

important pockets (4 and 9), which could account for its capacity to induce an immunological response.

Another important property for an immunogenic epitope is its location in the native protein. The epitope is located on the NA surface, providing accessibility for the Ab. According to 3D models, the predicted epitope is located at C-terminal domain and has an undefined secondary structure, which indicates that it is a loop located in the protruding region. The peptide possesses the important immunogenic properties of accessibility and protrusion.

Current research suggests that virtually any region on the exposed surface of a folded protein has the potential to serve as a B-cell epitope. Because polar residues are situated on the surface much more frequently than nonpolar residues, the regions of highest average polarity within a polypeptide sequence have the highest likelihood of being targets for Ab binding. The target peptide has 5 residues (3 Asp, 1 Glu, and 1 Lys) that have charges at pH 7.4 and can form electrostatic interactions and 7 residues that possess a polar group and can form hydrogen bonds. Thus, because of its hydrogen bonds, the peptide has enough side chain residues to maintain its stability and exposure properties in a hydrophobic environment.

According to peptide predictors and molecular modeling studies, the peptide is likely a continuous epitope that can function as a conformational epitope, which can then bind to rabbit Ab. Experimental data confirm that it is a linear epitope recognized by T-cell receptors. It is assumed that the only epitopes that are readily mimicked by synthetic peptides are continuous epitopes, corresponding to a sequence of 6–10 residues in a protein Ag [72]. The fact that sera from infected individuals (immunized with the native protein) also recognized the peptide indicates that it is a continuous B-cell epitope. The Ab induced by native proteins generally do not cross-react well with discontinuous native epitopes unless they recognize a continuous or sequential epitope on the native protein [73, 74]. Therefore, the current results strongly suggest that the epitope is sequential and located on the surface of the neuraminidase, which is in agreement with the theoretical data (Fig. 2).

The theoretical studies provide evidence that the peptide contains T-cell (MHC II) and B-cell epitopes. It is likely that the peptide possesses two epitopes: (1) a B-cell epitope (linear or continuous) that could correspond to the SWPDGAELPFTIDK segment and (2) a T-cell epitope (linear) that could correspond to the GNSDTVGW segment [75, 76]. It is possible that T cells and B cells have different specificities for the same epitope or that they have a specificity for distinct epitopes. There are examples in which T cells and Ab appear to have the same or very closely overlapping sites on a protein; however, specificity analyses indicate that the Ab and T-cell specificities are not identical. In the event of the existence of only one epitope, the B-cell receptor could protect the epitope from proteolytic enzymes (selective processing). Therefore, the epitope could be presented in association with the MHC protein on the surface of B cells to T cells [74]. The B-cell surface immunoglobulins take up the specific Ag with high affinity, internalize them by receptor-mediated endocytosis, and process them like any other Ag. Such protection from the proteolysis of Ag epitopes by bound Ab can be demonstrated in vitro [77].

Docking and MD simulations suggest that MHC II is able to recognize the epitope. The epitope–MHC II complex is stable over time, and this epitope could be recognized by helper T cells that control the switching to the IgG isotope. Moreover, there is indirect evidence that the peptide binds to MHC in vivo. When rabbits were immunized with the neuraminidase peptide, they produced specific antibodies of the IgG isotype. However, individuals naturally infected with the 2009 pandemic influenza A H1N1 virus produced antibodies of both the IgG (serum) and IgA isotypes (saliva). The production of IgG and IgA antibodies requires activated helper T cells that recognize the antigen (epitope T) in association with the MHC II protein on the surface of an antigen-presenting cell, such as B cells or dendritic cells. The production of IgG and IgA in response to the neuraminidase peptide indicates that helper T cells were activated by the peptide associated with the MHC II molecules.

Our results suggest that the immunological properties of the peptide could be used to develop a peptide-based vaccine. This excellent immunogen elicits specific cellular and humoral immunities, is located in a conserved region, and may induce antibodies that are cross-reactive to other influenza subtypes. However, further studies are needed to explore whether antibodies induced by the peptide can neutralize the infectivity of the virus and protect the host against infection. Thus, polyclonal or monoclonal antibodies to the peptide could be used in the diagnosis of infection by the influenza virus.

Conclusion

The current study demonstrates that in silico experiments are effective tools for the rational design of epitope vaccines for controlling the influenza A H1N1 virus. These experiments reduce the experimental evaluation necessary because only immunogenic epitopes are selected. Thus, the time and money invested in the design and development of epitope vaccines can be significantly reduced. Interestingly, our study indicates that the selected peptide is immunogenic and antigenic, inducing strong systemic (IgG) and mucosal (IgA) immune responses. Therefore, it should be a good candidate for the development of a peptide-based vaccine.

Acknowledgments The authors thank ICyTDF (PIRIVE09-9), CONACYT, and PIFI-SIP-COFAA/IPN for financial support and Teresita Rocio Cruz for technical support. We are grateful to Bruce Allan Larsen for reviewing the use of English. Veronica Briz was supported by the Fondo de Investigación Sanitaria (Spain) through the *Sara Borrell* program (CD9/00433). MB and LTL thank CONACYT for scholarships.

References

1. Yan S, Wu G. Evidence for cross-species infections and cross-subtype mutations in influenza a matrix proteins. Viral Immunol. 2010;23:105–11.
2. Hampson AW, Mackenzie JS. The influenza viruses. Med J Aust. 2006;185:S39–43.
3. Drake JW. Rates of spontaneous mutation among RNA viruses. Proc Natl Acad Sci USA. 1993;90:4171–5.
4. Nobusawa E, Sato K. Comparison of the mutation rates of human influenza A and B viruses. J Virol. 2006;80:3675–8.
5. LaRussa P. Pandemic novel 2009 H1N1 influenza: what have we learned? Semin Respir Crit Care Med. 2011;32:393–9.
6. Compans RW. Hemagglutination-inhibition: rapid assay for neuraminic acid-containing viruses. J Virol. 1974;14:1307–9.
7. Maeda Y, Hatta M, Takada A, Watanabe T, Goto H, Neumann G, Kawaoka Y. Live bivalent vaccine for parainfluenza and influenza virus infections. J Virol. 2005;79:6674–9.
8. Xie Y, Gong J, Li M, Fang H, Xu W. The medicinal potential of influenza virus surface proteins: hemagglutinin and neuraminidase. Curr Med Chem. 2011;18:1050–66.
9. Booy R, Brown LE, Grohmann GS, Macintyre CR. Pandemic vaccines: promises and pitfalls. Med J. 2006;185:S62–5.
10. Kawai R, Ito S, Aida T, Hattori H, Kimura T, Furukawa T, Mori K, Sanbuissho A, Kawada T. Evaluation of primary and secondary responses to a T-cell-dependent antigen, keyhole limpet hemocyanin, in rats. J Immunotoxicol. 2012 Sep 7. [Epub ahead of print].
11. Vivona S, Gardy JL, Ramachandran S, Brinkman FSL, Raghava GPS, Flower DR, Filippini F. Computer-aided biotechnology: from immunoinformatics to reverse vaccinology. Trends Biotechnol. 2008;26:190–200.
12. Ponomarenko J, Bui HH, Li W, Fusseder N, Bourne PE, Sette A, Peters B. ElliPro: a new structure-based tool for the prediction of antibody Epítopes. BMC Bioinf. 2008;9:514.
13. Khan JM, Ranganathan S. pDOCK: a new technique for rapid and accurate docking of peptide ligands to major histocompatibility complexes. Immun Res. 2010;6(Suppl 1):S2.
14. Cárdenas C, Bidon-Chanal A, Conejeros P, Arenas G, Marshall S, Luque FJ. Molecular modeling of class I and II alleles of the major histocompatibility complex in Salmo salar. J Comput Aided Mol Des. 2010;24:1035–51.
15. Zhang Q, Petersen HH, Ostergaard H, Ruf W, Olson AJ. Molecular dynamics simulations and functional characterization of the interactions of the PAR2 ectodomain with factor VIIa. Proteins. 2009;77:559–69.
16. Pérez-Padilla R, Fernández R, García-Sancho C, Franco-Marina F, Mondragón E, Volkow P. Demand for care and nosocomial infection rate during the first influenza AH1N1 2009 virus outbreak at a referral hospital in Mexico City. Salud Publica Mex. 2011;53:334–40.
17. Gille C, Frömmel C. STRAP: editor for structural alignments of proteins. Bioinformatics. 2001;17:377–8.
18. Arnold K, Bordoli L, Kopp J, Schwede T. The SWISS-MODEL workspace: a web-based environment for protein structure homology modelling. Bioinformatics. 2006;22:195–201.
19. Kiefer F, Arnold K, Künzli M, Bordoli L, Schwede T. The SWISS-MODEL repository and associated resources. Nucleic Acids Res. 2009;37:D387–92.
20. Peitsch MC. Protein modeling by E-mail. Nat Biotechnol. 1995;13:658–60.
21. Sali A, Blundell TL. Comparative protein modelling by satisfaction of spatial restraints. J Mol Biol. 1993;234:779–815.
22. Li Q, Qi J, Zhang W, Vavricka CJ, Shi Y, Wei J, Feng E, Shen J, Chen J, Liu D, He J, Yan J, Liu H, Jiang H, Teng M, Li X, Gao GF. The 2009 pandemic H1N1 neuraminidase N1 lacks the 150-cavity in its active site. Nat Struct Mol Biol. 2010;17:1266–8.
23. Moreno-Vargas L, Correa-Basurto J, Maroun RC, Fernández FJ. Homology modeling of the structure of acyl coA:isopenicillin 5 N-acyltransferase (IAT) from *Penicillium chrysogenum*. IAT 6 interaction studies with isopenicillin-N, combining molecular 7 dynamics simulations and docking. J Mol Model. 2012;18:1189–205.
24. Kim JH, Lim JW, Lee SW, Kim K, No KT. Ligand supported homology modeling and docking evaluation of CCR2: docked pose selection by consensus scoring. J Mol Model. 2011;17:2707–16.
25. Collins PJ, Haire LF, Lin YP, Liu J, Russell RJ, Walker PA, Skehel JJ, Martin SR, Hay AJ, Gamblin SJ. Crystal structures of oseltamivir-resistant influenza virus neuraminidase mutants. Nature. 2008;453:1258–62.
26. Singh H, Raghava GP. Propred: prediction of HLA-DR binding sites. Bioinformatic. 2001;17:1236–7.
27. Lata S, Bhasin M, Raghava GP. Application of machine learning techniques in predicting MHC binders. Methods Mol Biol. 2007;409:201–15.
28. Kulkarni-Kale U, Bhosle S, Kolaskar AS. CEP: a conformational epitope prediction server. Nucleic Acids Res. 2005;33:168–71.
29. Schanen BC, De Groot AS, Moise L, Ardito M, McClaine E, Martin W, Wittman V, Warren WL, Drake DR III. Coupling sensitive in vitro and in silico techniques to assess cross-reactive CD4(+) T cells against the swine-origin H1N1influenza virus. Vaccine. 2011;29:3299–309.
30. Southwood S, Sidney J, Kondo A, del Guercio MF, Appella E, Hoffman S, Kubo RT, Chesnut RW, Grey HM, Sette A. Several common HLA-DR types share largely overlapping peptide binding repertoires. J Immunol. 1998;160:3363–73.
31. Morris GM, Goodsell DS, Halliday RS, Huey R, Hart WE. Automated docking using a Lamarckian genetic algorithm and an empirical binding free energy function. J Comput Chem. 1998;19:1639–62.
32. Patronov A, Dimitrov I, Flower DR, Doytchinova I. Peptide binding prediction for the human class II MHC allele HLA-DP2: a molecular docking approach. BMC Struct Biol. 2011;11:32.
33. Phillips JC, Braun R, Wang W, Gumbart J, Tajkhorshid E, Villa E, Chipot C, Skeel RD, Kalé L, Schulten K. Scalable molecular dynamics with NAMD. J Comput Chem. 2005;16:1781–802.
34. MacKerell AD Jr, Bashford D, Bellott M, Dunbrack RL Jr, Evanseck J, Field MJ, Fischer S, Gao J, Guo H, Ha S, Joseph D, Kuchnir L, Kuczera K, Lau FTK, Mattos C, Michnick S, Ngo T, Nguyen DT, Prodhom B, Reiher IWE, Roux B, Schlenkrich M, Smith J, Stote R, Straub J, Watanabe M, Wiorkiewicz-Kuczera J, Yin D, Karplus M. All-atom empirical potential for molecular modeling and dynamics studies of proteins. J Phys Chem B. 1998;102:3586–616.
35. Glykos NM. Carma: a molecular dynamics analysis program. J Comput Chem. 2006;27:1765–8.
36. Humphrey W, Dalke A, Schulten K. VMD: visual molecular dynamics. J Mol Graph. 1996;14:33–8, 27–8.
37. Rivera-Aguilar V, Hernández-Martínez D, Rojas-Hernández S, Oliver-Aguillón G, Tsutsumi V, Herrera-González N, Campos-

Rodríguez R. Immunoblot analysis of IgA antibodies to Naegleria fowleri in human saliva and serum. Parasitol Res. 2001;86:775–80.
38. Edgar RC. Optimizing substitution matrix choice and gap parameters for sequence alignment. BMC Bioinf. 2009;10:396.
39. Johnson LS, Eddy SR, Portugaly E. Hidden Markov model speed heuristic and iterative HMM search procedure. BMC Bioinf. 2010;11:431.
40. Hamelin ME, Baz M, Abed Y, Couture C, Joubert P, Beaulieu E, Bellerose N, Plante M, Mallett C, Schumer G, Kobinger GP, Boivin G. Oseltamivir-resistant pandemic A/H1N1 virus is as virulent as its wild-type counterpart in mice and ferrets. PLoS Pathog. 2010;6:e1001015.
41. Colman PM. Influenza virus neuraminidase: structure, antibodies, and inhibitors. Protein Sci. 1994;3:1687–96.
42. Okomo-Adhiambo M, Nguyen HT, Sleeman K, Sheu TG, Deyde VM, Garten RJ, Xu X, Shaw MW, Klimov AI, Gubareva LV. Host cell selection of influenza neuraminidase variants: implications for drug resistance monitoring in A(H1N1) viruses. Antivir Res. 2010;85:381–8.
43. Ghosh A, Nandy A, Nandy P. Computational analysis and determination of a highly conserved surface exposed segment in H5N1 avian flu and H1N1 swine flu neuraminidase. BMC Struct Biol. 2010;10:6.
44. Jiang W, Boder ET. High-throughput engineering and analysis of peptide binding to class II MHC. Proc Natl Acad Sci USA. 2010;107:13258–63.
45. Zimic M, Gutiérrez AH, Gilman RH, López C, Quiliano M, Evangelista W, Gonzales A, García HH, Sheen P. Immunoinformatics prediction of linear epitopes from Taenia solium TSOL18. Bioinformation. 2011;6:271–4.
46. Flower DR, Macdonald IK, Ramakrishnan K, Davies MN, Doytchinova IA. Computer aided selection of candidate vaccine Antigens. Immunome Res. 2010;6(suppl2):S1.
47. Jørgensen KW, Buus S, Nielsen M. Structural properties of MHC class II ligands, implications for the prediction of MHC class II epitopes. PLoS ONE. 2010;5:e15877.
48. Yang J, Aslimovska L, Glaubitz C. Molecular dynamics of proteorhodopsin in lipid bilayers by solid-state NMR. J Am Chem Soc. 2011;133:4874–81.
49. Frömmel C. Use of the averaged mutation rate in pieces of protein sequences to predict the location of antigenic determinants. J Theor Biol. 1988;132:171–7.
50. Ding X, Jiang L, Ke C, Yang Z, Lei C, Cao K, Xu J, Xu L, Yang X, Zhang Y, Huang P, Huang W, Zhu X, He Z, Liu L, Li J, Yuan J, Wu J, Tang X, Li M. Amino acid sequence analysis and identification of mutations under positive selection in hemagglutinin of 2009 influenza A (H1N1) isolates. Virus Genes. 2010;41:329–40.
51. Sinigaglia F, Hammer J. Rules for peptide binding to MHC class II molecules. APMIS. 1994;102:241–8.
52. Ofek G, Guenaga FJ, Schief WR, Skinner J, Baker D, Wyatt R, Kwong PD. Elicitation of structure-specific antibodies by epitope scaffolds. Proc Natl Acad Sci USA. 2010;107:17880–7.
53. Muszkat KA, Schechter B, Sela M. Aromatic side-chain interactions as the origin of immunological diversity in the TyrTyrGluGlu and TyrGluTyrGlu epitopes: NMR and fluorescence evidence. Int Immunol. 1993;5:591–7.
54. Ménez R, Bossus M, Muller BH, Sibaï G, Dalbon P, Ducancel F, Jolivet-Reynaud C, Stura EA. Crystal structure of a hydrophobic immunodominant antigenic site on hepatitis C virus core protein complexed to monoclonal antibody 19D9D6. J Immunol. 2003;170:1917–24.
55. Bordner AJ. Towards universal structure-based prediction of class II MHC epitopes for diverse allotypes. PLoS ONE. 2010;5:e14383.
56. Stern LJ, Brown JH, Jardetzky TS, Gorga JC, Urban RG, Strominger JL, Wiley DC. Crystal structure of the human class II MHC protein HLA-DR1 complexed with an influenza virus peptide. Nature. 1994;17:215–21.
57. Amaro RE, Baron R, McCammon JA. An improved relaxed complex scheme for receptor flexibility in computer-aided drug design. J Comput Aided Mol Des. 2008;22:693–705.
58. Tzakos AG, Fuchs P, van Nuland NA, Troganis A, Tselios T, Deraos S, Matsoukas J, Gerothanassis IP, Bonvin AM. NMR and molecular dynamics studies of an autoimmune myelin basic protein peptide and its antagonist Structural implications for the MHC II (I-Au)–peptide complex from docking calculations. Eur J Biochem. 2004;271:3399–413.
59. Norberto de Souza O, Ornstein RL. Molecular dynamics simulations of a protein-protein dimer: particle-mesh Ewald electrostatic model yields far superior results to standard cutoff model. J Biomol Struct Dyn. 1999;16:1205–18.
60. Yin J, Bowen D, Southerland WM. Barnase thermal titration via molecular dynamics simulations: detection of early denaturation sites. J Mol Graph Model. 2006;24:233–43.
61. Camacho CJ, Katsumata Y, Ascherman DP. Structural and thermodynamic approach to peptide immunogenicity. PLoS Comput Biol. 2008;4(11):e1000231.
62. Nielsen M, Lund O, Buus S, Lundegaard C. MHC class II epitope predictive algorithms. Immunology. 2010;130:319–28.
63. Painter CA, Cruz A, Lopez GE, Stern LJ, Zavala-Ruiz Z. Model for the peptide-free conformation of class II MHC proteins. PLoS ONE. 2008;3(6):e2403.
64. James EA, Moustakas AK, Bui J, Nouv R, Papadopoulos GK, Kwok WW. The binding of antigenic peptides to HLA-DR is influenced by interactions between pocket 6 and pocket 9. J Immunol. 2009;183:3249–58.
65. Langton BC, Mackewicz CE, Wan AM, Andria ML, Benjamini E. Structural features of an antigen required for cellular interactions and for T cell activation in a MHC-restricted response. J Immunol. 1988;141:447–56.
66. Benjamin DC, Berzofsky JA, East IJ, Gurd FR, Hannum C, Leach SJ, Margoliash E, Michael JG, Miller A, Prager EM, et al. The antigenic structure of proteins: a reappraisal. Annu Rev Immunol. 1984;2:67–101.
67. Madhumathi J, Prince PR, Anugraha G, Kiran P, Rao DN, Reddy MV, Kaliraj P. Identification and characterization of nematode specific protective epitopes of Brugia malayi TRX towards development of synthetic vaccine construct for lymphatic filariasis. Vaccine. 2010 [Epub ahead of print].
68. Benkirane N, Friede M, Guichard G, Briand JP, Van Regenmortel MH, Muller S. Antigenicity and immunogenicity of modified synthetic peptides containing D-amino acid residues. J Biol Chem. 1993;268:26279–85.
69. Pandiaraja P, Arunkumar C, Hoti SL, Rao DN, Kaliraj P. Evaluation of synthetic peptides of WbSXP-1 for the diagnosis of human lymphatic filariasis. Diagn Microbiol Infect Dis. 2010;68:410–5.
70. Klein J, Horejsi V. Immunology. 2nd ed. Oxford: Blackwell Science; 1977. p. 396.
71. McConnell I, Lachmann PJ, Hobart MJ. Restoration of specific immunological virginity. Nature. 1974;250:113–6.
72. Van Regenmortel MH. Antigenicity and immunogenicity of synthetic peptides. Biologicals. 2001;29:209–13.
73. Berzofsky JA, Buckenmeyer GK, Hicks G, Gurd FR, Feldmann RJ, Minna J. Topographic antigenic determinants recognized by monoclonal antibodies to sperm whale myoglobin. J Biol Chem. 1982;257:3189–98.
74. Berzofsky JA, Berkower I. Immunogenicity and antigen structure. In: Paul W, editor. Fundamental immunology. 4th ed. Philadelphia: Lippincott-Raven; 1999. p. 651–99.

75. Berkower I, Kawamura H, Matis LA, Berzofsky JA. T cell clones to two major T cell epitopes of myoglobin: effect of I-A/I-E restriction on epitope dominance. J Immunol. 1985;135:2628–34.
76. Berkower I, Buckenmeyer GK, Berzofsky JA. Molecular mapping of a histocompatibility-restricted immunodominant T cell epitope with synthetic and natural peptides: implications for T cell antigenic structure. J Immunol. 1986;136:2498–503.
77. Jemmerson R, Paterson Y. Mapping epitopes on a protein antigen by the proteolysis of antigen-antibody complexes. Science. 1986; 232:1001–4.